Mechanism and Dynamics of Oxygen Storage/Release in a Pt/CeO_2-ZrO_2 Catalyst Studied using Time-resolved XAFS Analysis

CeO_2-ZrO_2 (CZ) materials can store oxygen under oxygen-excess conditions and release it under oxygen-deficient conditions. Due to their high oxygen storage/release capacities (OSC) they are widely used as promoters in three-way automobile catalysts. We have succeeded for the first time in characterizing the electronic and structural transformations of a Pt-promoted CZ catalyst with ordered Ce and Zr ions during the oxygen storage/release processes at 573-773 K using real-time energy-dispersive XAFS, and discover new chemistry.

The CeO_2-ZrO_2 (CZ) material with the highest oxygen storage/release capacity (OSC) is a CeO_2-ZrO_2 solid solution, which possesses an atomically homogeneous and ordered arrangement of Ce and Zr ions, assigned to a κ-$Ce_2Zr_2O_8$ fluorite phase (Fig. 1) [1]. A total of 89% of the Ce ions in the Pt-promoted κ-$Ce_2Zr_2O_8$ are available for the oxygen storage/release process, in contrast to CeO_2 itself which has an OSC value of 2%. The κ-$Ce_2Zr_2O_8$ transforms to pyrochlore $Ce_2Zr_2O_7$ under reducing conditions during the working state, and the $Ce_2Zr_2O_7$ returns to κ-$Ce_2Zr_2O_8$ under oxidizing conditions. The real-time study of the dynamics of these processes is relevant to understanding the OSC functionality of the CZ materials, and has been achieved using time-resolved XAFS for the first time [2]. In pyrochlore $Ce_2Zr_2O_7$, the Ce ions are in the +3 charge state and 8-fold coordinated, while the Zr ions are +4 and 6-fold coordinated. In the transformation between κ-$Ce_2Zr_2O_8$ and $Ce_2Zr_2O_7$, the Zr sites show a change in coordinated oxygen number with no change in valency, whereas the Ce sites show a change in valency with no change in coordination number. Time-resolved energy-dispersive XAFS spectra at the Ce L_3-edge and the Zr K-edge with energy ranges of 5.67-5.87 keV and 17.8-18.8 keV respectively were recorded at the NW2A beamline at the PF-AR. Si(111) (Ce L_3-edge) and Si(311) (Zr K-edge) bent-crystal polychromators (Bragg-type) were utilized to obtain elliptical optics for focusing the incident X-rays at the sample.

By means of the real-time measurements we have succeeded in characterizing the electronic and structural transformations of the Pt-promoted CZ catalyst with ordered arrangement of Ce and Zr ions during the oxygen storage/release processes at 573-773 K [2]. Isosbestic points were observed in all of the XANES spectra except for the first 0.9 s and the last 2 s of the transformation, indicating that the majority of the κ-$Ce_2Zr_2O_8$ transforms directly to pyrochlore $Ce_2Zr_2O_7$. The change in Ce valency at 773 K was almost complete after only 1 s (with 90% of the Ce ions active in oxygen release and 80% in oxygen storage). Thus the oxygen storage/release process is a dynamic event involving $Ce_2Zr_2O_x$ nanoparticles, which are 200 nm in dimension.

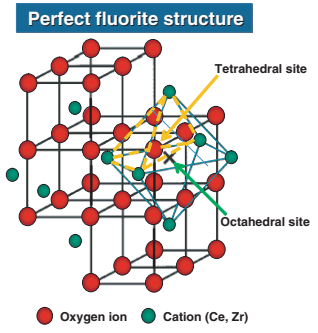

Figure 1
Tetrahedral (T_d) and octahedral (O_h) sites in the fluorite $Ce_2Zr_2O_8$ structure based on the oxygen sub-lattice (O_h sites are not occupied). Oxygen atoms begin to migrate by moving from T_d sites to O_h sites.

To elucidate the dynamics of the Zr-O bond formation/breaking in the CZ solid solution during the OSC function, the change of the coordination sphere around the Zr ions was monitored using both energy-dispersive XANES and EXAFS at the Zr K-edge with a time resolution of 2 ms. Figure 2 (a) shows real-time k^3-weighted energy-dispersive EXAFS Fourier transforms for Pt/$Ce_2Zr_2O_8$ during the oxygen release process at 773 K. The changes in the coordination number and bond distance of Zr-O were successfully analyzed although the obtained distances are averaged. The results at 773 K are plotted in Fig. 2 (b). During the oxygen storage process (Fig. 2 (c)) the coordination number and bond distance slowly increased over a period of 5 s, reaching values of 7.0 and 0.214 nm respectively. Only small increases are seen during the first 1 s, in contrast to the change in Ce valence, and $Ce_2Zr_2O_7$ transformed to $Ce_2Zr_2O_8$ after 6 s. During the oxygen release process the coordination number decreased from eight to seven in the first 1 s, followed by a gentle decrease to six. The bond distance rapidly shortened from 0.220 nm to 0.214 nm within the first 1 s, followed by a continuous decrease to 0.208 nm at the onset of the change in the coordination number.

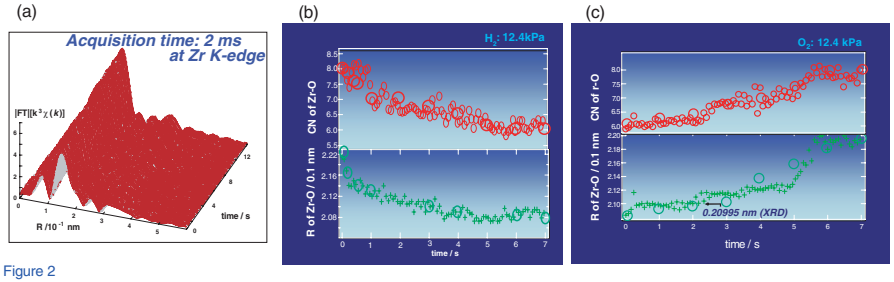

Figure 2
Real-time DXAFS at 2 ms time resolution at the Zr K-edge.
(a) Serial Fourier transformed k^3-weighted EXAFS functions during the oxygen release process at 773 K. (b) Time profiles of the coordination number and bond distance of Zr-O during the oxygen release process at 773 K. (c) Time profiles of the coordination number and bond distance of Zr-O during the oxygen storage process at 773 K. Large circles in the time profiles: 100 ms acquisition for comparison.

The fractions of $Ce_2Zr_2O_8$ and $Ce_2Zr_2O_7$ during the oxygen storage and release processes at 573, 673 and 773 K were also determined by a linear combination analysis of the energy-dispersive XANES spectra at the Zr K-edge. For example, the Ce L_3-edge XANES analysis for the oxygen release process demonstrates that 90% of the Ce^{4+} ions in $Ce_2Zr_2O_8$ were reduced within 1 s at 773 K, whereas it took 4 s for 90% transformation at the Zr sites as deduced from the Zr K-edge XANES analysis.

Based on the time-resolved XAFS analysis, we conclude that the electronic and structural transformations at the Ce and Zr sites during the oxygen storage/release processes do not synchronize with each other in the solid solution. In both the storage and release processes a change in the valence of the Ce sites preceded a structural transformation at the Zr sites, making or breaking Zr-O bonds. The dynamics at the Zr sites observed with energy-dispersive XAFS characterization involves changes in the local structure, the number of coordinated oxygen atoms, and oxygen diffusion. This new aspect may be explained by valence fluctuation at the Ce sites and charge redistribution due to a change of the lattice constant involving a modification of the Ce-O distance. This study has successfully revealed for the first time the dynamics and roles of the Ce and Zr ions in the industrially practical Pt/CeO_2-ZrO_2 catalyst, demonstrating the promise of the application of dynamic XAFS to a variety of mixed oxide catalyses.

REFERENCES

[1] A. Suda, Y. Ukyo, H. Sobukawa and M. Sugiura, *J. Ceram. Soc. Jpn.*, **110** (2002)126
[2] T. Yamamoto, A. Suzuki, Y. Nagai, T. Tanabe, F. Dong, Y. Inada, M. Nomura, M. Tada and Y. Iwasawa, *Angew. Chem. Int. Ed.*, **46** (2007) 9253.

BEAMLINE

AR-NW2A

M. Tada and Y. Iwasawa (The Univ. Tokyo)

Catalyst Development for Energy-efficient Syngas Production from Natural Gas in Gas-to-liquid Processes by Oxidative Steam Reforming of Methane

Oxidative steam reforming of methane is a promising syngas production method, which will contribute to energy-efficient production of liquid fuels from natural gas. Conventional catalysts cannot be applied to the oxidative steam reforming of methane because of serious problems of hot-spot formation. The purpose of this study is catalyst development for the catalysts with high resistance to hot-spot formation by an effective modification of Ni catalysts with very small amount of noble metals. As a result, it is important that Pt and Pd atoms should be located preferably on the surface of bimetallic particles.

Much attention has been paid to sulfur-free transportation fuels produced by gas-to-liquid (GTL) processes relating to the petroleum price soaring, exhaustion of petroleum, and environmental problems on exhaust gases [1]. The GTL process consists of the production of synthesis gas (syngas, mixture of CO and H_2) from natural gas, whose main component is CH_4, and Fischer-Tropsch synthesis from the synthesis gas ($nCO+2nH_2 \rightarrow (CH_2)_n+nH_2O$). Conventional syngas production method is steam reforming ($CH_4+H_2O \rightarrow CO+3H_2$), which is an energy-consuming process. Recently, oxidative steam reforming of natural gas, where oxygen is also introduced to the catalyst bed, is expected as a more energy-efficient syngas production method. Here, hot-spot formation is a serious problem which can cause the severe catalyst deactivation by very high temperature. Our purpose is development of catalyst with high resistance to hot-spot formation.

The temperature profile of the catalyst bed and IR thermograph (Figs. 1(a) and (b)) clearly showed a very high temperature region at the inlet of the catalyst bed and a much lower temperature region in the downstream were observed over Ni(2.6), where a number in the parenthesis represents the loading amount (wt%) of metal components. The hot-spot formation and large temperature gradient make the operation difficult. The Pt(0.1) exhibited a flatter temperature profile than Ni(2.6). However, the catalytic activity was not enough. The temperature profile on the Pt(0.1)+Ni(2.6) catalyst was similar to that on the Ni(2.6), which indicates that the additive effect of Pt introduced by the co-impregnation method is small. In contrast, the temperature gradient on the Pt(0.1)/Ni(2.6) is much smaller than those of the other three catalysts, which means that the additive effect of Pt introduced by the sequential impregnation method is remarkable in spite of very small molar ratio of Pt to Ni [2]. The Pt(0.1)/Ni(2.6) and Pt(0.1)+Ni(2.6) were characterized by Pt L_3- and Ni *K*-edge EXAFS, FTIR of CO adsorption, TEM, amount of H_2 adsorption, and temperature programmed reduction. A possible model structure of Pt-Ni bimetallic particles is also illustrated in Fig. 1(c). The additive effect of Pt can be caused by surface Pt atoms on the Pt-Ni bimetallic particles, which is strongly influenced by the preparation methods. In addition, similar behavior was observed in the case of the modification with Pd [3].

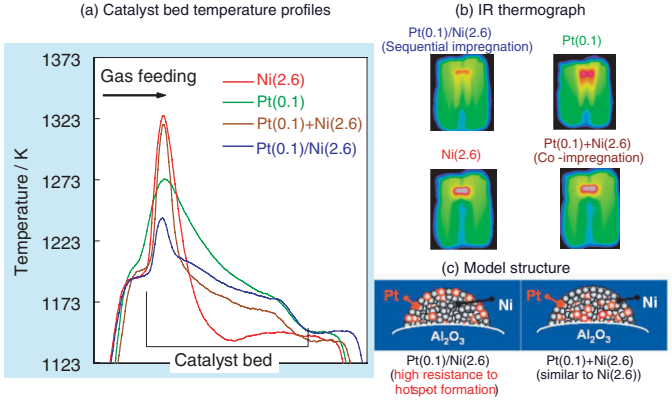

Figure 1
Oxidative steam reforming of methane over Pt-Ni bimetallic catalysts.
Reaction conditions: $CH_4/H_2O/O_2/Ar$ = 4/3/2/1, total flow rate=430 cm^3/min, 0.1 MPa, cat. weight=0.08 g, 1123 K.

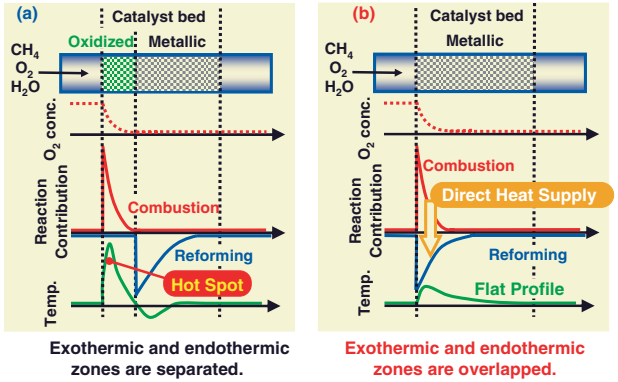

Figure 2
Hot-spot formation mechanism of monometallic NI catalysts (a) and suppression mechanism of hot-spot formation of Pt/Ni and Pd/Ni bimetallic catalysts (b).

Figure 2 depicts the hot-spot formation mechanism on Ni catalysts and suppression mechanism of hot-spot formation on Ni catalysts modified with Pt and Pd [1]. Hot-spot formation over the Ni catalysts at the inlet is due to exothermic combustion reaction over the oxidized Ni catalysts with O_2 in the gas phase (Fig. 2(a)). In particular, the oxidized Ni species loses the reforming activity and solely has the combustion activity. On the other hand, at the outlet of the catalyst bed where no oxygen remains, the Ni species are maintained in the metallic state; the Ni species presents the reforming activity. In this reaction zone, only the endothermic reaction proceeds and the catalyst bed temperature decreases, which results in a large temperature gradient. In contrast, on the Pt/Ni and Pd/Ni catalysts, the reduced state of the species is maintained even in the presence of oxygen in the gas phase, and the reduced species can also serve as the active site for the methane reforming as well as the combustion (Fig. 2(b)). The endothermic reforming reaction can contribute to a temperature decrease at the inlet of the catalyst bed, which is connected to flat temperature profile and suppression of hot-spot formation.

The EXAFS analysis gave the ratio of noble metal atoms located at the surface of bimetallic particles, and the ratio is closely related to the suppression of hot spot formation. The modification of Ni catalysts with small amount of Pt and Pd gave the excellent property of noble metal catalysts with higher loading amount, which results in saving of the usage of noble metals and decrease of the catalyst cost.

REFERENCES

[1] K. Tomishige, *J. Jpn. Petrol. Inst.*, **50** (2007) 287.
[2] B.T. Li, S. Kado, Y. Mukainakano, T. Miyazawa, T. Miyao, S. Naito, K. Okumura, K. Kunimori and K. Tomishige, *J. Catal.*, **245** (2007) 144.
[3] Y. Mukainakano, B.T. Li, S. Kado, T. Miyazawa, K. Okumura, T. Miyao, S. Naito, K. Kunimori and K. Tomishige, *Appl. Catal. A*, **318** (2007) 252.

BEAMLINE

9C and AR-NW10A

K. Tomishige[1], K. Okumura[2], T. Miyao[3] ([1]Univ. Tsukuba, [2]Tottori Univ. [3]Kanagawa Univ.)

XAFS Analysis of the Specific Interaction of Cu^+ in CuMFI with Dinitrogen Molecule at Room Temperature

There are few materials that can adsorb dinitrogen (N_2) molecules easily and safely around room temperature. In the present work, we found that a copper-ion-exchanged MFI-type zeolite (CuMFI), which exhibits an extremely efficient adsorption of the N_2 molecule even at room temperature, could be successfully prepared by ion exchange in an aqueous solution of $Cu(CH_3COO)_2$ containing a component of NH_4CH_3COO. The structure of the adsorbed N_2 species on Cu^+ in MFI was determined by XAFS (X-ray absorption fine structure) measurements. The three-coordinated monovalent copper ions formed in MFI act as the active sites for N_2 adsorption at room temperature, with the N_2 molecules adsorbing linearly. The results provide significant information on the development of materials with catalytic functions of efficient N_2-fixation catalysts, N_2-activation catalysts, as well as NO_x decomposition catalysts.

Recently, there has been a renewal of interest in the fields of fundamental research into the adsorption, activation, and fixation of small molecules, in particular N_2, which is relatively inert [1]. However, there are few materials that can adsorb N_2 molecules easily, safely, and rapidly at temperatures around 300 K. Two candidates exhibiting N_2-adsorption are metallic Li and Mg, however the reaction of N_2 with these materials is not fast at room temperature. In addition, these materials are hazardous under ambient conditions. We have discovered for the first time [2] that a copper-ion-exchanged mordenite sample, which has an ion exchange capacity beyond 100% (i.e., a nonstoichiometrically ion-exchanged material), exhibits a prominent adsorption feature for N_2 molecules even at 300 K. The present work is intended to develop a preparation method for a copper-ion-exchanged MFI-type zeolite sample (CuMFI: Scheme 1) endowed with an activity against N_2 molecules at 300 K, and also to obtain further information on the states of the active centers for N_2 adsorption. As a result, we have succeeded in the preparation of CuMFI, which exhibits extremely efficient adsorption of N_2 molecule at room temperature, by ion exchange in an aqueous solution of $Cu(CH_3COO)_2$ containing a component of NH_4CH_3COO [3,4]. The prepared material is stable and safe. The ion-exchange method used here has the following unique characteristics; first, the copper-ion exchange takes place exclusively on the ion-exchangeable site that acts as the active site for N_2 adsorption,

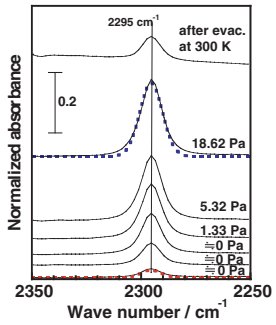

Figure 1
IR spectra of N_2 species adsorbed on CuMFI at 300 K under various pressures. The fitted (single component) IR spectra of the samples are represented by the dotted line.

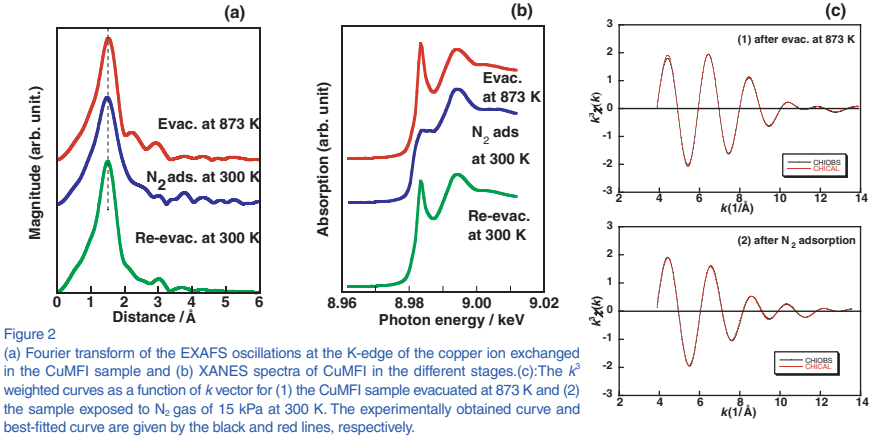

Figure 2
(a) Fourier transform of the EXAFS oscillations at the K-edge of the copper ion exchanged in the CuMFI sample and (b) XANES spectra of CuMFI in the different stages.(c):The k^3 weighted curves as a function of k vector for (1) the CuMFI sample evacuated at 873 K and (2) the sample exposed to N_2 gas of 15 kPa at 300 K. The experimentally obtained curve and best-fitted curve are given by the black and red lines, respectively.

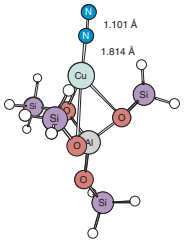

Figure 3
Optimized structure for the N_2 species adsorbed on three-coordinated copper ion which was obtained on the basis of the DFT method.

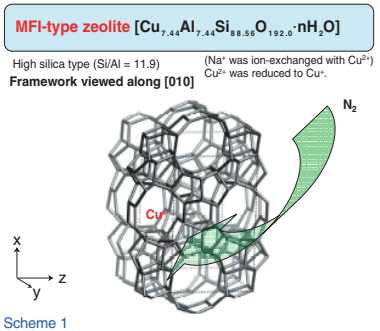

Scheme 1
Schematic view of the CuMFI sample.

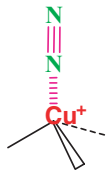

Scheme 2
Adsorption model of N_2 on the monovalent copper ion formed in MFI.

and secondly, the extent of the reduction of the divalent copper-ion exchanged attains a value as high as 88% after evacuation of the sample at 873 K. On this sample, N_2 was efficiently adsorbed, resulting in the appearance of an IR band due to the adsorbed N_2 molecules (Fig. 1). These observations were rationalized as showing that site-selective ion exchange with copper ions occurs, and that the divalent copper-ions exchanged in this way can be reduced easily and efficiently to monovalent ions [3-5]. In addition, CuMFI exhibits a high efficiency for N_2 adsorption at 300 K where the monovalent copper ions act as adsorption sites; approximately 86% of them are effective for N_2 adsorption. In this case, the heats of adsorption of N_2 also show large values, ranging from 87 to 60 kJ mol^{-1}.

The XAFS method is a very powerful and indispensable tool for the characterization of the surface states of catalysts, and is also the best method for obtaining structural information related to the active centers in various catalytic and adsorption processes. The measurements of the XAFS spectra of CuMFI were carried out at BL-9C (Figs. 2(a) and 2(b)). From this experiment, the coordination environment of the copper ions adsorbing N_2 for this sample was clarified by EXAFS analysis, and the resultant data were well fitted as shown in Fig. 2(c) (EXAFS and their fitting data: N(Cu-O) = 2.7 ± 0.2, N(Cu-N) = 1.1 ± 0.1; r(Cu-O) = 1.97 ± 0.01Å, r(Cu-N) = 1.91 ± 0.01Å). XANES spectra also indicate that the monovalent copper ion is the active center. By a combination with various other spectroscopic methods, such as IR, diffuse reflectance UV-Vis, and photoluminescence spectra, it was concluded that the N_2 molecules were adsorbed linearly at 300 K on the three-coordinated monovalent copper ions formed in MFI. The final adsorption model obtained is given in Scheme 2. The density functional theory (DFT) calculation was also applied for the proposed N_2-adsorption model (Fig. 3), and the resultant IR and adsorption heat values were evaluated to be 2305 cm^{-1} and 101 kJ mol^{-1} for the N_2 species adsorbed on the three-coordinated copper ion; both values are in fair agreement with the experimental values.

To clarify the active center for the N_2 adsorption, we also examined the effects of the Si/Al ratio of the mother MFI on the N_2 adsorption phenomena at 300 K and on the ion-exchange feature of the CuMFI. The CuMFI sample with an Si/Al ratio of 19.8, which had been prepared by using a $Cu(C_2H_5COO)_2$ solution, exhibited extremely efficient N_2 adsorption in terms of both the number of adsorbed molecules and its energetic behavior, as compared to samples with other Si/Al ratios and/or with other ion-exchange solutions [6].

In this way, the XAFS spectra provide significant structural and electronic information on the copper-ion exchanged in MFI which plays the important role in the N_2 adsorption. These results are expected to be important in developing more efficient materials for N_2-fixantion or N_2-activation, as well as for NO_x decomposition [7-10].

REFERENCES

[1] H.-J. Himmel and M. Reiher, *Angew. Chem. Int. Ed.*, **45** (2006) 6264.
[2] Y. Kuroda, S.-I. Konno, K. Morimoto and Y. Yoshikawa, *J. Chem. Soc., Chem. Commun.*, (1993) 18.
[3] A. Itadani, M. Tanaka, T. Mori, M. Nagao, H. Kobayashi and Y. Kuroda, *J. Phys. Chem. C*, **111** (2007) 12011.
[4] A. Itadani, H. Sugiyama, M. Tanaka, T. Mori, M. Nagao and Y. Kuroda, *J. Phys. Chem. C*, **111** (2007) 16701.
[5] T. Mori, A. Itadani, E. Tabuchi, Y. Sogo, R. Kumashiro, M. Nagao and Y. Kuroda, *Phys. Chem. Chem. Phys.*, **10** (2008) 1203.
[6] A. Itadani, M. Tanaka, Y. Kuroda and M. Nagao, *New J. Chem.*, **31** (2007) 1681.
[7] M. Iwamoto, H. Furukawa, Y. Mine, F. Uemura, S. Mikuriya and S. Kagawa, *J. Chem. Soc., Chem. Commun.*, **1986** 1272.
[8] M. Iwamoto and H. Hamada, *Catal. Today*, **10** (1991) 57.
[9] M. Iwamoto and H. Yahiro, *Catal. Today*, **22** (1994) 5.
[10] Y. Kuroda and M. Iwamoto, *Topic Catal.*, **28** (2004) 111.

BEAMLINE

9C

A. Itadani[1], M. Tanaka[1], H. Kobayashi[2] and Y. Kuroda[1] ([1]Okayama Univ., [2]Kyoto Inst. of Tech.)

In-Situ XAFS Studies of Au Particle Formation by Photoreduction in Polymer Solutions

The photo-reduction formation mechanisms of gold particles in an aqueous ethanol solution of $HAuCl_4$ with poly(*N*-vinyl-2-pyrrolidone) (PVP) have been investigated using transmission electron microscopy (TEM) and in-situ X-ray absorption fine structure (XAFS) analyses. It was found that the reduction of $AuCl_2^-$ to Au^0 atoms is a slower process than that of $AuCl_4^-$ to $AuCl_2^-$, and proceeds concurrently with the association of Au^0 atoms to form seed Au particles with diameters between 5.5 and 30 Å.

For the preparation of small metal particles, metal ions are often chemically reduced in protective media. As the protective media for colloidal metal particles in aqueous solutions, water-soluble polymers such as poly(vinyl alcohol) and poly(*N*-vinyl-2-pyrrolidone) (PVP) have often been used [1, 2]. The use of a polymeric matrix allows control of the nucleation and growth of the metal particles, which imparts new properties to the polymeric materials. Various studies on the preparation of Au particles by photo-irradiation have been carried out, and it is well-known that preparative photo-irradiation is a powerful technique for regulating size and shape in the particle formation process. However the formation mechanisms of Au particles have not yet been elucidated, and must be investigated in order to improve the preparative technique for the control of particle size and shape.

In-situ XAFS measurements at the Au-L_3 edge were performed at BL-10B and BL-7C. Controlled UV light with a UV-30 cut filter was used to investigate the mechanisms of Au particle formation during photo-irradiation. The sample solutions contained $AuCl_4^-$ in quartz cells sealed with Kapton films, and were continuously stirred and photo-irradiated using a mercury lamp during the in-situ XAFS measurements. The absorption spectra were recorded in the transmission mode at room temperature, and data analysis was performed using the REX2000 program (Rigaku Corp.). The k^3-weighted EXAFS function was Fourier transformed into r space over a range of typically between 3 and 16 $Å^{-1}$.

Figure 1(a) shows the Fourier transforms of the Au-L_3 edge spectra for the Au colloidal solutions stabilized by PVP before and after photo-reduction. The peak around 2.0 Å observed for the sample before photo-reduction is assigned to the Au-Cl bond in $AuCl_4^-$, and that observed around 2.8 Å after long-duration photo-irradiation is assigned to the Au-Au metallic bond in Au particles. A noticeable decrease in peak intensity for the Au-Cl bond is seen below 30 min, although the peak attributed to the Au-Au bond appears only after 30 min, indicating the onset for the formation of Au particles. It is noted that between 30 and 120 min the peak intensity for the Au-Cl bond of the photo-irradiated sample is nearly the same intensity as that for the Au^+-Cl^- bond in the AuCl powder sample, the spectrum of which is shown in Fig. 1(b). It is also observed that the peak intensity for the Au-Au bond becomes gradually higher with increasing reduction time, while the peak for the Au-Cl bond decreases only until the reduction time reaches 360 min. Thus the reduction of $AuCl_2^-$ to Au^0 atoms and the association of Au^0 atoms to form seed Au particles (with the coordination number of the Au-Au bonds less than 10 and an estimated particle diameter between 5.5 and 30 Å) proceed concurrently. After long photo-irradiation times, the seed Au particles are activated to create larger Au particles. The TEM observations indicate that the slow progression of Au particle growth continues, and larger particles (with diameters larger than 500 Å) form under dark conditions after photo-irradiation for 750 min [3].

In summary, an Au-L_3 XAFS analysis of colloidal dispersions of Au particles in PVP solutions revealed that the electronic structure of the photo-irradiated samples is composed of three stable states, Au^{3+} (a reactant, $AuCl_4^-$), Au^+ (stable product, $AuCl_2^-$), and Au^0 atoms (or Au particles produced from Au^0 atoms). The reduction of $AuCl_2^-$ to Au^0 atoms is a slower process than that of $AuCl_4^-$ to $AuCl_2^-$, and proceeds concurrently during photo-irradiation with the association of Au^0 atoms to form seed Au particles.

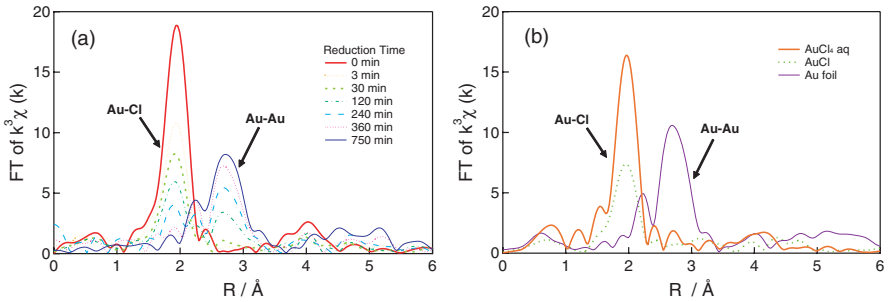

Figure 1
In-situ EXAFS results: Fourier transforms of the Au-L_3 edge spectra for (a) Au colloidal solutions stabilized by PVP and (b) AuCl powder, $HAuCl_4 \cdot 3H_2O$ aqueous solution and Au foil. (a) shows the time dependence of the spectra during photo-reduction over a period of 750 min.

REFERENCES

[1] M. Harada, N. Toshima, K. Yoshida and S. Isoda, *J. Colloid Interface Sci.*, **283** (2005) 64.
[2] M. Harada and H. Einaga, *Langmuir*, **22** (2006) 2371.
[3] M. Harada and H. Einaga, *Langmuir*, **23** (2007) 6536.

BEAMLINE

10B and 7C

M. Harada[1] and H. Einaga[2] ([1]Nara Women's Univ., [2]Kyushu Univ.)

The Structure of Hydrous Mg-Silicate Melts under High Pressure and High Temperature by In Situ X-Ray Diffraction

We performed in situ X-ray diffraction experiments to investigate the structural changes which occur as hydrous Mg-silicate melts under high pressure and high temperature. We used a new encapsulation method, a DIA multi-anvil apparatus and synchrotron radiation. For each hydrous melt composition, the first sharp diffraction peaks, *FSDP*s, which reflect the periodicity of silicate network ordering, showed lengthening or no shortening between 3 and 5 GPa in spite of the compression. This behavior results from changes in the polymerization of the silicate network caused by the transition of dominant water speciation from Si-OH to Mg-OH. This change can help explain the physicochemical properties of hydrous silicate melt at high pressure.

It is widely known that the presence of water has dramatic effects on the physicochemical properties of silicate melt, such as density, viscosity, and phase relations. A particularly interesting example can be seen in the hydrous MgO-SiO_2-H_2O system under high-pressure conditions. It is well understood that the melt composition at low pressures is enriched in SiO_2 (up to 5 GPa for the Mg_2SiO_4-$MgSiO_3$-H_2O system). In contrast, an abrupt change from a SiO_2-rich to a MgO-rich composition begins at higher pressure (see e.g., [1]). The atomic scale structural mechanism for this evolution with pressure has not been investigated with in situ observations until the present study.

The starting materials were prepared from mixtures of powdered $Mg(OH)_2$ brucite and SiO_2, with molar proportions of 1 : 1, 2 : 1 and 3 : 2 for hydrous enstatite (En), hydrous En_{50}-Fo_{50}, and forsterite (Fo). The H_2O contents by weight were 15.2%, 18.3%, and 20.4%, respectively. High-pressure and high-temperature X-ray diffraction experiments were performed at the PF-AR NE5C beamline using the MAX80 DIA-type press and polychromatic X-ray energies. To maintain the hydrous silicate melt and ensure high X-ray transparency at high pressure and temperature, we have developed a new encapsulation method using single-crystal diamond and platinum (see e.g., [2]).

The X-ray interference functions for each hydrous Mg-silicate melt are shown in Fig. 1. The first peaks (*FSDP*) are indicated with arrows. The *FSDP* for silicate melt and glass is often related to the silicate network structure (see e.g., [3]), which can be illustrated by linkages of corner-sharing SiO_4 tetrahedra. The position of the *FSDP* reflects the periodicity of the silicate network ordering with the distance of $2\pi/Q$ [Å] ($Q = 4\pi E\sin\theta/12.398$ [$Å^{-1}$], where Q, E and θ are the scattering vector, the energy of the X-ray, and the Bragg angle, respectively). The pressure dependence of the position of the *FSDP* for each composition melt is shown in Fig. 2. The position shifts to lower distances up to ~3 GPa in each hydrous Mg-silicate melt, suggesting a significant decrease in the periodicity of the silicate network. In contrast, at pressures between 3 and 5 GPa the *FSDP* position either moves to the longer distance side or does not move with increasing compression. In particular, a lengthening of the periodicity at pressures between 3 and 5 GPa is obvious for the Mg_2SiO_4 composition. This discontinuous behavior in the periodicity of the silicate network is not observed for anhydrous $MgSiO_3$ melt [4], also shown in Fig. 2.

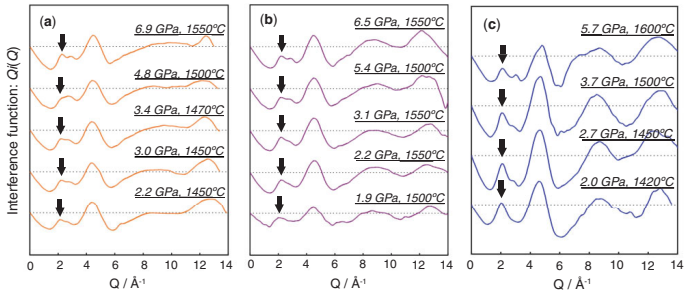

Figure 1
Interference functions $Qi(Q)$ for Mg_2SiO_4-H_2O (a), Mg_2SiO_4-$MgSiO_3$-H_2O (b) and $MgSiO_3$-H_2O (c). Arrows indicate the position of the first sharp diffraction peak, *FSDP*, for each $Qi(Q)$.

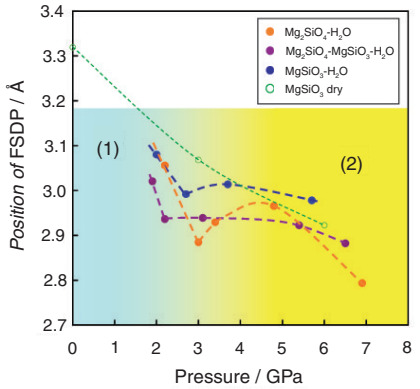

Figure 2
Pressure dependence of the positions of *FSDP*. The region (1) hatched with blue indicates the region in which SiOH water speciation is dominant in the silicate melt. The region (2) hatched with yellow indicates the region in which MgOH water speciation is dominant. The data for anhydrous $MgSiO_3$ melt is taken from [4].

The structural change in the silicate network can be explained as a transition of the dominant water speciation in the melt. The decrease in periodicity up to 3 GPa is ascribed to a de-polymerization of water on the silicate network, which can be described schematically by the following relationship.

$$SiOSi + H_2O \rightarrow 2SiOH \quad (1),$$

where "SiOSi" and "SiOH" indicate the silicate network, in the melt and the water speciation produced by dividing the silicate network, respectively [5]. The silicic melt generation in the lower pressure region, as described above, has been regarded as the result of this water solubility mechanism. On the other hand, the lengthening of the silicate network ordering at pressures between 3 and 5 GPa can be interpreted as the following relation, as proposed by a recent NMR study (see e.g., [7]).

$$SiOH + SiOMg \rightarrow MgOH + SiOSi \quad (2).$$

The "MgOH" on the right hand side is a new water speciation, reported in [6]. This relation suggests that repolymerization of the silicate network (SiOSi) occurs, with a change in preference of the hydroxyl component from SiO_2 to MgO at high pressure. In this mechanism, the MgO component plays an important role in the repolymerization. In fact, the lengthening of the silicate network ordering is obvious in the Mg_2SiO_4 melt, which has the highest MgO content in this study. Moreover, this water solubility mechanism offers a promising explanation for the genesis of MgO-rich melt under hydrous conditions at high pressure.

REFERENCES

[1] T. Inoue, *Phys. Earth Planet. Inter.*, **85** (1994) 237.
[2] A. Yamada, T. Inoue, S. Urakawa, K. Funakoshi, N. Funamori, T. Kikegawa, H. Ohfuji and T. Irifune, *Geophys. Res. Lett.*, **34** (2007) L10303.
[3] Y. Inamura, Y. Katayama, W. Utsumi and K. Funakoshi, *Phys. Rev. Lett.*, **93** (2004) 015501.
[4] N. Funamori, S. Yamamoto, T. Yagi and T. Kikegawa, *J. Geophys. Res.*, **109** (2004) B03203.
[5] E.M. Stolper, *Geochim. Cosmochim. Acta.*, **46** (1982) 2609.
[6] X. Xue and M. Kanzaki, *Geochim. Cosmochim. Acta.*, **68** (2004) 5027.

BEAMLINE

AR-NE5C

A. Yamada[1, 2], T. Inoue[2] and T. Kikegawa[3] ([1]Univ. of California, Davis, [2]Ehime Univ., [3]KEK-PF)